AIAA JOURNAL
Vol. 39, No. 5, May 2001

Structural Dynamics of Stiffened Plates with Piezoceramic Sensors and Actuators

Kenneth M. Newbury* and Donald J. Leo†
Virginia Polytechnic Institute and State University, Blacksburg, Virginia 24061-0261

A dynamic model of a stiffened plate, developed for the purpose of analyzing the coupling between piezoceramic transducers and the plate dynamics, is presented. The model is based on Hamilton's principle and discretized with a polynomial expansion of the transverse plate vibration. The effects of eccentric stiffeners, piezoceramic transducers, and point masses located on the plate are accounted for in the model. To validate the model, the results of numerical simulations are compared with experiments on a rectangular aluminum plate with one eccentric stiffener and simply supported boundary conditions. The model accurately predicts the first seven natural frequencies and mode shapes of the plate as well as the coupling between piezoceramic transducers and the plate vibration. A study of the plate natural frequencies and transducer coupling over a range of stiffener heights reveals that for geometries with slight asymmetries and near repeated eigenvalues the corresponding mode shapes are very sensitive to small changes in stiffener height. For the structure studied in this work, the sensitivity of the mode shapes caused the piezoceramic transducer modal strain energy fraction for the fourth mode to increase by 140% with only an 8% increase in stiffener height. Over the same range of stiffener heights, the piezoceramic transducer modal strain energy fraction for the symmetric structure's fourth mode only changed by 5%.

Nomenclature

A	=	cross-sectional area
$A_{mn}(t)$	=	expansion coefficient
a	=	plate length
$\boldsymbol{a}$	=	vector of expansion coefficients
a_{mn}	=	expansion coefficient
b	=	plate width
C, c	=	boundary condition spring constant (torsional spring)
C_{11}, C_{12}, C_{44}	=	lead zirconate titanate (PZT) elastic constants
D	=	bending stiffness of the plate
d_{31}	=	piezoelectric coefficient
E	=	elastic modulus
F	=	impact magnitude
G	=	shear modulus
h	=	height (z direction)
I	=	stiffener moment of inertia
K, k	=	boundary condition spring constant (linear spring)
$\boldsymbol{K}$	=	stiffness matrix
K_t	=	torsional constant of stiffener
L	=	Lagrangian
$\boldsymbol{M}$	=	mass matrix
m_{PtMass}	=	point mass
n	=	number of degrees of freedom
$\boldsymbol{Q}$	=	force vector
Q_k	=	external forces
q_k	=	generalized coordinates
r	=	ratio of the plate length to width
T	=	kinetic energy
t_{stiff}	=	stiffener thickness
U^f_{PZT}	=	fractional modal strain energy in the PZTs (nondimensional)
U^f_{stiff}	=	fractional strain energy in the stiffener (nondimensional)
V	=	potential energy
V_{in}	=	applied voltage
V_{out}	=	output voltage
W	=	out-of-plane displacement
x	=	in-plane coordinate
y	=	in-plane coordinate
z	=	out-of-plane coordinate
α	=	nondimensional in-plane coordinate (x direction)
β	=	nondimensional in-plane coordinate (y direction)
δT	=	kinetic energy of the system
δW	=	virtual work
ε_0	=	permittivity of free space
κ	=	relative permittivity
ν	=	Poisson's ratio
ρ	=	density
$\boldsymbol{\Phi}$	=	vector of trial function products
ω	=	angular frequency

Introduction

STIFFENED plates are widely used in civil, marine, and aerospace structures because of their high strength-to-weight ratio. A stiffened plate structure typically consists of a plate that is reinforced by attaching beams to one surface. Both the load-carrying ability and the dynamics of the stiffened plate are affected by the geometry and material properties of the plate and stiffeners. An understanding of the structural dynamics of stiffened plates is important to researchers in fields such as vibration control and acoustic radiation. In addition, the ability to evaluate sensor and actuator performance is beneficial in active control applications.

For a specified plate and stiffener layout the fundamental frequency, mode shapes, and the modal spacing will depend on the properties of the stiffeners. The majority of previous research involving stiffened plate vibration has been focused on finding approximations for the natural frequencies as a function of the stiffener properties using either the Rayleigh–Ritz method or a finite element method. For example, in one of the earlier works on stiffened plate vibration, Kirk[1] used the Rayleigh–Ritz method with simply supported plate mode shapes as trial functions to find the approximate natural frequency of the (1,1) mode and the (1,2) mode of a simply supported, thin, isotropic plate with a single stiffener. Laura and Gutierrez[2] investigated the vibration of rectangular plates with a particular set of boundary conditions and varying stiffener length using the Rayleigh–Ritz method and approximating the fundamental

Received 15 March 2000; revision received 16 August 2000; accepted for publication 15 October 2000.

*Graduate Research Assistant, Center for Intelligent Material Systems and Structures, Mechanical Engineering Department. Student Member AIAA.

†Assistant Professor, Center for Intelligent Material Systems and Structures, Mechanical Engineering Department. Member AIAA.

mode shape using a polynomial function. Numerous finite element studies[3–8] have also been performed on stiffened plates, some to determine natural frequencies, others to calculate static deflection with an out-of-plane load.

Natural frequency approximations are usually sufficient for applications in which the primary concern is avoiding a structural resonance. In noise and vibration control applications, though, the mode shapes play an equally important role in the design of effective passive and active treatments. It is well known that structural sound radiation is related to the radiation efficiency of the vibration modes.[9] This concept has been extended in recent years to the study of radiation modes[10] as a means of determining which modes are dominant in the acoustic response of a structure. Mode shapes also play a central role in the design of passive damping treatments using the modal strain energy approach,[11] and they are directly related to the amount of energy dissipated in passive shunts.[12]

The primary contribution of this work is a general Rayleigh–Ritz model that can accurately predict the natural frequencies and mode shapes of a stiffened structure with surface bonded piezoceramic transducers. The Rayleigh–Ritz model is based on a polynomial expansion of the out-of-plane displacement of the plate. The discretized model results in a mass and stiffness matrix that incorporates the energy terms as a result of the plate, stiffener, boundary conditions, piezoceramic transducers, and any point masses located on the structure.

Piezoceramic actuators and sensors have gained considerable attention in recent years as a result of their ability to be integrated directly into the structure. In the past a variety of methods have been developed for modeling-induced strain actuation of structures. In earlier studies[13–15] assumed stress or strain distributions were analyzed to determine statically equivalent forces or moments that were then used to represent the actuator's influence on the structure. Even in dynamic analyses, these forces or moments were assumed to be independent of frequency. In most of the early models, the added mass and stiffness caused by the actuator were also neglected. Later approaches[16–19] have incorporated the dynamics of the interaction between the actuator and the host structure as well as the change in the host structure's dynamics resulting from the presence of the actuator. The later models have been shown to yield more accurate results for dynamic analyses.

In the present work the effects of piezoceramic sensors and actuators are added directly to the kinetic and potential energy terms of the plate and stiffener. Modeling the piezoceramics in this manner incorporates the effects of localized stiffening on the response of the material and the plate. Variations in the mode shape and natural frequency caused by the properties of the piezoceramic are naturally included in this formulation.

This paper is organized as follows. A Rayleigh–Ritz model is developed from the Hamiltonian of the plate, stiffener, and piezoceramic elements. Mode shapes and natural frequencies are verified experimentally on a simply supported plate with a single stiffener. Analyses are performed on the variation in the natural frequencies and mode shapes as a function of stiffener height. The modal strain energy fraction in the piezoceramic elements is analyzed to determine control authority as a function of stiffener properties. The final section summarizes the work and presents the major conclusions.

In the Nomenclature, subscripts of a symbol (except for indices) indicate the component to which a symbol pertains; for example, ρ_{plt} is the density of the plate material.

Model Development

The model developed in this work is based on the extended Hamilton's principle[20]

$$\int_{t_1}^{t_2} (\delta T + \delta W)\, \mathrm{d}t = 0$$

$$\delta q_k(t_1) = \delta q_k(t_2) = 0, \qquad k = 1, 2, \ldots, n \tag{1}$$

If both the energy and work terms in Eq. (1) can be described using a set of time-varying coordinates and their velocities only, then Eq. (1) can be represented by Lagrange's equations of motion:

$$\frac{\mathrm{d}}{\mathrm{d}t}\left(\frac{\partial L}{\partial \dot{q}_k}\right) - \frac{\partial L}{\partial q_k} = Q_k, \qquad k = 1, 2, \ldots, n \tag{2}$$

There are basically two approaches to describing the motion of the stiffener and the plate. In one approach the midplane of the plate is assumed to be the neutral surface, and the strain field in the stiffener and plate are described entirely in terms of the out-of-plane displacement of the plate. Membrane forces in the plate and axial forces in the stiffener(s) that result from the eccentricity of the actual neutral surface are ignored. In the other approach no assumptions are made about the location of the neutral surface, and the in-plane displacements are described with independent degrees of freedom. In our work the first approach is used because it has been demonstrated[21] that if the stiffeners are sparse the assumption that the neutral axis is coincident with the midplane of the plate does not lead to significant errors. The geometries that will be studied using this model will be limited to only a few stiffeners. Another method sometimes used to simplify modeling of a stiffened plate is to replace it with an "equivalent" orthotropic unstiffened plate.[21–23] Although this method can be effective when the spacing between the stiffeners is small compared with the distance between vibration nodes, it cannot accurately predict the structural modes when the stiffeners are sparse, unevenly spaced, or significantly varied in size. Also, it has been shown[21] that this approach will lead to errors in high-order modes. The severity of the errors and at what frequency they begin to appear depend on the particular approximations used in calculating the equivalent orthotropic plate parameters.

For our work the out-of-plane displacement of the plate is approximated using the set of polynomial trial functions with time-varying contribution coefficients:

$$W(x, y, t) = \sum_{m=0}^{N}\sum_{n=0}^{N} A_{mn}(t)\left(\frac{2x}{a}\right)^m\left(\frac{2y}{b}\right)^n \tag{3}$$

This expansion is the same as one used by Charette and Berry[16] for the study of unstiffened plate vibration. This approximation will allow the expression of the kinetic energy, potential energy, and virtual work in terms of the coefficients A_{mn} and their first time derivatives. The coordinate system is shown in Fig. 1. If the contribution coefficients are assumed to be periodic in time,

$$A_{mn} = a_{mn} e^{j\omega t} \tag{4}$$

Lagrange's equations of motion for the system will yield the system of constant coefficient linear equations

$$(-\omega^2 \boldsymbol{M} + \boldsymbol{K})\boldsymbol{a} = \boldsymbol{Q} \tag{5}$$

which is an N^2 degree-of-freedom model of the system that can be solved for the approximate system response. The system mass matrix $\boldsymbol{M}$ and stiffness matrix $\boldsymbol{K}$ will be the sum of contributions from the individual components of the structure: plate, stiffener(s), piezoceramic transducer(s), and point mass(es). In this work the

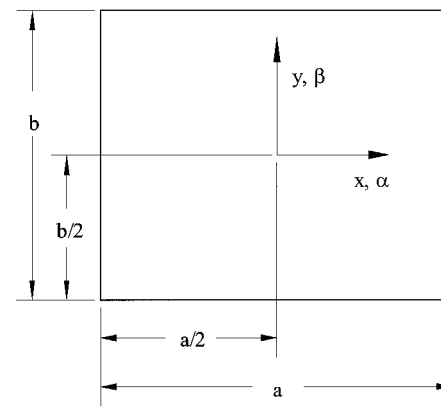

Fig. 1 Plate coordinate system.

force vector $\boldsymbol{Q}$ is derived for both voltage excitation of a surface-bonded piezoceramic transducer and for an out-of-plane point impact. Modal analysis is used to solve for the system response. In brief, this method consists of first solving the homogeneous (free vibration) problem to obtain a modal model of the system. Modal damping values either are assumed or are estimated from experimental data. The force vector is then transformed into modal coordinates, and the modal responses calculated. These modal responses are transformed into physical coordinates $\boldsymbol{a}$, and the expansion terms in Eq. (3) are summed to find the approximate system response $W(x, y, t)$. For convenience, we will express the expansion in Eq. (3) in a more compact form:

$$W = \boldsymbol{a}^T \boldsymbol{\Phi} e^{j\omega t}$$

where

$$\boldsymbol{\Phi} = [\alpha^0\beta^0 \quad \alpha^0\beta^1, \ldots, \alpha^0\beta^N \quad \alpha^1\beta^0, \ldots, \alpha^N\beta^N]^T$$

$$\alpha = 2x/a, \qquad \beta = 2y/b, \qquad r = a/b \tag{6}$$

The spatial coordinates in the directions of the plate length and width have been nondimensionalized and are represented by α and β.

Structural Model

The mass and stiffness matrices are derived from the energy terms for the plate, stiffener(s), piezoceramic transducer, and a point mass located on the plate surface. As with the model developed by Charette and Berry,[16] the derivation of the plate stiffness matrix is based on the small deflection theory of thin plates, which allows all of the significant stresses and strains to be written in terms of the motion of the midplane of the plate W. The thin plate assumptions are as follows[24]:

1) The strains at the midplane of the plate are zero.

2) Normal strain in the z direction can be neglected, and the normal stress in the z direction is small enough compared with the normal stresses in the x and y directions so that it can be ignored in the stress-strain relations.

3) Normals to the midplane of the plate remain normal to this plane after bending. This assumption means that out-of-plane shear strains are small enough that they can be neglected.

With these assumptions the stiffness matrix for the plate is

$$\boldsymbol{K}_{\text{plt}} = \frac{4D}{ra^2} \iint_{A_{\text{plt}}} \left[\boldsymbol{\Phi}_{\alpha\alpha}\boldsymbol{\Phi}_{\alpha\alpha}^T + r^4\boldsymbol{\Phi}_{\beta\beta}\boldsymbol{\Phi}_{\beta\beta}^T + \nu r^2\left(\boldsymbol{\Phi}_{\alpha\alpha}\boldsymbol{\Phi}_{\beta\beta}^T + \boldsymbol{\Phi}_{\beta\beta}\boldsymbol{\Phi}_{\alpha\alpha}^T\right) + 2r^2(1-\nu)\boldsymbol{\Phi}_{\alpha\beta}\boldsymbol{\Phi}_{\alpha\beta}^T\right] \mathrm{d}\alpha\, \mathrm{d}\beta \tag{7}$$

where

$$D = \frac{E_{\text{plt}}(h_{\text{plt}})^3}{12(1-\nu^2)} \tag{8}$$

The mass matrix for the plate is

$$\boldsymbol{M}_{\text{plt}} = \rho_{\text{plt}} h_{\text{plt}} \frac{a^2}{4r} \iint_{A_{\text{plt}}} \boldsymbol{\Phi}\boldsymbol{\Phi}^T \,\mathrm{d}\alpha\, \mathrm{d}\beta \tag{9}$$

The mass and stiffness contributions of a stiffener oriented parallel to the α axis are

$$\boldsymbol{K}_{\text{stiff}} = E_{\text{stiff}} I \frac{8}{a^3} \int_{-1}^{1} \boldsymbol{\Phi}_{\alpha\alpha}\boldsymbol{\Phi}_{\alpha\alpha}^T \,\mathrm{d}\alpha + K_t G \frac{8r^2}{a^3} \int_{-1}^{1} \boldsymbol{\Phi}_{\alpha\beta}\boldsymbol{\Phi}_{\alpha\beta}^T \,\mathrm{d}\alpha \qquad \text{with } \beta = 0 \tag{10}$$

$$\boldsymbol{M}_{\text{stiff}} = \rho_{\text{stiff}} h_{\text{stiff}} t_{\text{stiff}} \frac{a}{2} \int_{-1}^{1} \boldsymbol{\Phi}\boldsymbol{\Phi}^T \,\mathrm{d}\alpha + \rho_{\text{stiff}} I \frac{2r^2}{a} \int_{-1}^{1} \boldsymbol{\Phi}_{\beta}\boldsymbol{\Phi}_{\beta}^T \,\mathrm{d}\alpha \qquad \text{with } \beta = 0 \tag{11}$$

Note that the stiffener moment of inertia I is computed about the assumed neutral surface, the midplane of the plate. The torsional constant is

$$K_t = \frac{h_{\text{stiff}} t_{\text{stiff}}^3}{3}\left(1 - 0.630\frac{t_{\text{stiff}}}{h_{\text{stiff}}} + 0.052\frac{t_{\text{stiff}}^5}{h_{\text{stiff}}^5}\right) \tag{12}$$

for a rectangular cross section. The mass and stiffness matrices for a stiffener parallel to the β axis are similar.

The mass and stiffness matrices of a piezoceramic transducer bonded to the plate surface are

$$\boldsymbol{K}_{\text{pzt}} = \left[\frac{h_{\text{pzt}}^2}{12} + \frac{(h_{\text{plt}} + h_{\text{pzt}})^2}{4}\right] h_{\text{pzt}} \frac{4}{a^2 r} \times \iint_{A_{\text{pzt}}} \left(C_{11}\left[\boldsymbol{\Phi}_{\alpha\alpha}\boldsymbol{\Phi}_{\alpha\alpha}^T + r^2\boldsymbol{\Phi}_{\beta\beta}\boldsymbol{\Phi}_{\beta\beta}^T\right] + C_{12}r^2\left[\boldsymbol{\Phi}_{\alpha\alpha}\boldsymbol{\Phi}_{\beta\beta}^T + \boldsymbol{\Phi}_{\beta\beta}\boldsymbol{\Phi}_{\alpha\alpha}^T\right] + C_{44}4r^2\boldsymbol{\Phi}_{\alpha\beta}\boldsymbol{\Phi}_{\alpha\beta}^T\right) \mathrm{d}\alpha\, \mathrm{d}\beta \tag{13}$$

$$\boldsymbol{M}_{\text{pzt}} = \frac{\rho_{\text{pzt}} h_{\text{pzt}} a^2}{4r} \iint_{A_{\text{pzt}}} \boldsymbol{\Phi}\boldsymbol{\Phi}^T \,\mathrm{d}\alpha\, \mathrm{d}\beta \tag{14}$$

The elastic constants of the transducer are

$$C_{11} = \frac{E_{1,\text{pzt}}}{1-\nu_{\text{pzt}}^2}, \qquad C_{12} = \frac{\nu_{\text{pzt}} E_{1,\text{pzt}}}{1-\nu_{\text{pzt}}^2}$$

$$C_{44} = \frac{1}{2}(C_{11} - C_{12}) = \frac{E_{1,\text{pzt}}}{2(1+\nu_{\text{pzt}})} \tag{15}$$

Point masses are also modeled to account for the effects of transducers, such as accelerometers, used to measure plate response. The mass matrix caused by a point mass located at (x_m, y_m) is

$$\boldsymbol{M}_{\text{PtMass}} = m_{\text{PtMass}} \boldsymbol{\Phi}(x_m, y_m) \boldsymbol{\Phi}^T(x_m, y_m) \tag{16}$$

To allow modeling of a variety of boundary conditions, the structure's boundary is represented by massless linear springs perpendicular to the plate and massless torsional springs. By varying the spring constants, the model can represent free, clamped, and simply supported, as well as boundary conditions between these extremes. The boundary conditions will contribute only to the structure's stiffness matrix. The spring constants K and C in units of force/length^2 and force · length/rad · length are nondimensionalized with respect to the plate stiffness and length by the expressions

$$k = Ka^3/D, \qquad c = Ca/D \tag{17}$$

The stiffness matrix corresponding to the $\beta = -1$ boundary of the plate is

$$\boldsymbol{K}_{\text{bc1}} = \frac{kD}{2a^2} \int_{-1}^{1} \boldsymbol{\Phi}(\alpha, \beta = -1)\boldsymbol{\Phi}^T(\alpha, \beta = -1) \,\mathrm{d}\alpha + \frac{2Dcr^2}{a^2} \int_{-1}^{1} \boldsymbol{\Phi}_{\beta}(\alpha, \beta = -1)\boldsymbol{\Phi}_{\beta}^T(\alpha, \beta = -1) \,\mathrm{d}\alpha \tag{18}$$

The development of the stiffness matrix contributions for the other edges is similar and will not be shown.

The mass and stiffness matrices for the entire structure are calculated by adding the contributions from each component of the structure:

$$\boldsymbol{M} = \boldsymbol{M}_{\text{plt}} + \boldsymbol{M}_{\text{stiff}} + \boldsymbol{M}_{\text{pzt}} + \boldsymbol{M}_{\text{PtMass}}$$

$$\boldsymbol{K} = \boldsymbol{K}_{\text{plt}} + \boldsymbol{K}_{\text{stiff}} + \boldsymbol{K}_{\text{pzt}} + \boldsymbol{K}_{\text{bc's}} \tag{19}$$

The left-hand side of Eq. (5) is now complete, and the free vibration problem can be solved.

Forcing Functions and Sensor Equations

Two types of excitation are considered in this work: concentrated impact loads that are perpendicular to the plate and induced in-plane strains resulting from electrical excitation of the piezoceramic actuator(s). An impact load is represented by an impulsive force acting at a single point on the plate. The force vector $\boldsymbol{Q}_{\text{PtForce}}$ is found by differentiating the work that corresponds to a displacement at the point of the applied force with respect to the expansion coefficients $\boldsymbol{a}$:

$$\boldsymbol{Q}_{\text{PtForce}} = \frac{\partial W}{\partial \boldsymbol{a}} = F\boldsymbol{\Phi}(x_F, y_F) \tag{20}$$

Using the same technique, the force vector corresponding to voltage excitation of the piezoceramic actuator is

$$\boldsymbol{Q}_{\text{pzt}} = -\frac{V_{\text{in}} d_{31}}{2r}(C_{11} + C_{12})(h_{\text{pzt}} + h_{\text{plt}}) \times \iint_{A_{\text{pzt}}} \left(\boldsymbol{\Phi}_{\alpha\alpha} + r^2\boldsymbol{\Phi}_{\beta\beta}\right) \mathrm{d}\alpha\, \mathrm{d}\beta \tag{21}$$

Note that perfect bonding between the transducer and the plate is assumed.

Because of the piezoelectric effect, a piezoceramic transducer can also be used as a sensor. The expression for the voltage output is

$$V_{\text{out}} = -\frac{d_{31} h_{\text{pzt}}}{2r\kappa\epsilon_0 A_{\text{pzt}}}(C_{11} + C_{12})(h_{\text{pzt}} + h_{\text{plt}})\, \boldsymbol{a}^T \times \iint_{A_{\text{pzt}}} \left(\boldsymbol{\Phi}_{\alpha\alpha} + r^2\boldsymbol{\Phi}_{\beta\beta}\right) \mathrm{d}\alpha\, \mathrm{d}\beta \tag{22}$$

Note that the open-circuit voltage output is based on both the strain field in the transducer, which results from the displacement of the plate, and the transducer material properties.

Experimental Validation

The stiffened plate model was experimentally verified for the case of an aluminum plate (Fig. 2) with one eccentric stiffener and two surface-bonded lead zirconate titanate piezoceramic wafers (PZTs). The aluminum stiffener was bonded along the long centerline of the plate with epoxy. Simply supported boundary conditions were simulated by machining a groove near the perimeter of the plate from each side. The outer edges of the plate (outside the grooves) were clamped to a relatively stiff and massive fixture. The area inside the machined grooves was a (nearly) simply supported plate.

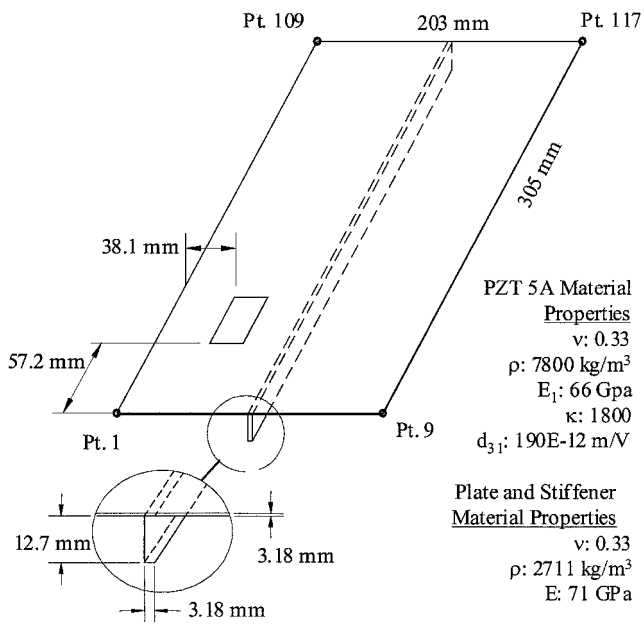

Fig. 2 Plate used for model validation experiments.

Table 1 Natural frequency comparison (experimental modal analysis vs model)

Mode	Frequency, Hz: Experiment	Model	Error, %	Shape
1	338	342	1.2	(1,1)
2	803	802	−0.1	(1,2)
3	894	935	4.6	(2,1)
4	1042	1041	−0.1	(2,2)
5	1442	1435	−0.5	(3,2)
6	1491	1543	3.5	(3,1)
7	1625	1610	−0.9	(1,3)

Data points were located by marking an evenly spaced 117 point grid on the plate. The 25.4 × 38.1 × 0.25 mm PZTs were bonded to opposite sides of the plate at the center of one of the plate quadrants. Orientation of the PZTs was such that an applied voltage resulted in a pure moment load on the plate. A modal analysis was performed by measuring response at a single location and exciting the structure at the 117 data points with an instrumented hammer. Plate response was measured using a laser interferometer, and an FFT analyzer was used to calculate frequency responses up to 2 kHz. Postprocessing for the modal analysis was performed using a commercial software package.

Natural Frequency and Mode Shape Analysis

To verify the modes predicted by the model, an experimental modal analysis was performed. The experimental and predicted frequencies agreed to within 5% for the first seven modes, and the model predicted the correct mode shapes. Table 1 summarizes the measured natural frequencies, the predicted natural frequencies, and the mode shapes for the first seven (all of the sub-2-kHz) modes. The rectangular plate mode shapes are denoted by the number of half-sine waves along the x and y axes, respectively; for example, plots of a few low-order mode shapes (see Ref. 20, p. 438).

Response Analysis

A collocated PZT sensor-actuator transfer function was used to verify the model's ability to predict the coupling between the PZTs and the plate vibration. The experimental and simulated transfer functions are shown in Fig. 3. In general, the agreement is good. However, the model does overpredict the natural frequencies of the first (1,1), third (2,1), and the sixth (3,1) modes by a few percent (Table 1). This is attributed to two factors. First, the model development is based on the assumption that the neutral axis is coincident with the midsurface of the plate. For a plate with eccentric stiffeners, this assumption results in a slight overprediction of the bending stiffness perpendicular to the stiffener, the magnitude of the error depending on the relative dimensions of the plate and stiffener. Second, the model does not account for the finite stiffness of the epoxy used to bond the stiffener to the plate. The compliance of the epoxy reduces the effectiveness of the stiffener on the experimental plate. Multiplication of the stiffener's contribution ($\boldsymbol{K}_{\text{stiff}}$) to the total stiffness matrix by 0.90 reduced the average percent error of the first seven modes from 1.1 to 0.2%.

Stiffened Plate Dynamics

The model described in this paper was used to investigate several features of the stiffened plate dynamics as the stiffener dimensions were varied. Also studied (as a function of stiffener dimensions) were the abilities of PZTs in two different locations to couple into the stiffened plate vibration.

To nondimensionalize the size of the stiffener relative to the plate, the strain energy of the stiffener is expressed as a fraction of the total strain energy in the stiffened plate for the case of pure bending perpendicular to the α axis. This type of displacement is represented by the trial functions in which $\boldsymbol{\Phi}_\beta = 0$, allowing integration with respect to β in Eq. (7). The resulting expression for the strain energy fraction is

$$U^f_{\text{stiff}} = \frac{EI(8/a^3)}{EI(8/a^3) + (8D/ra^2)} \tag{23}$$

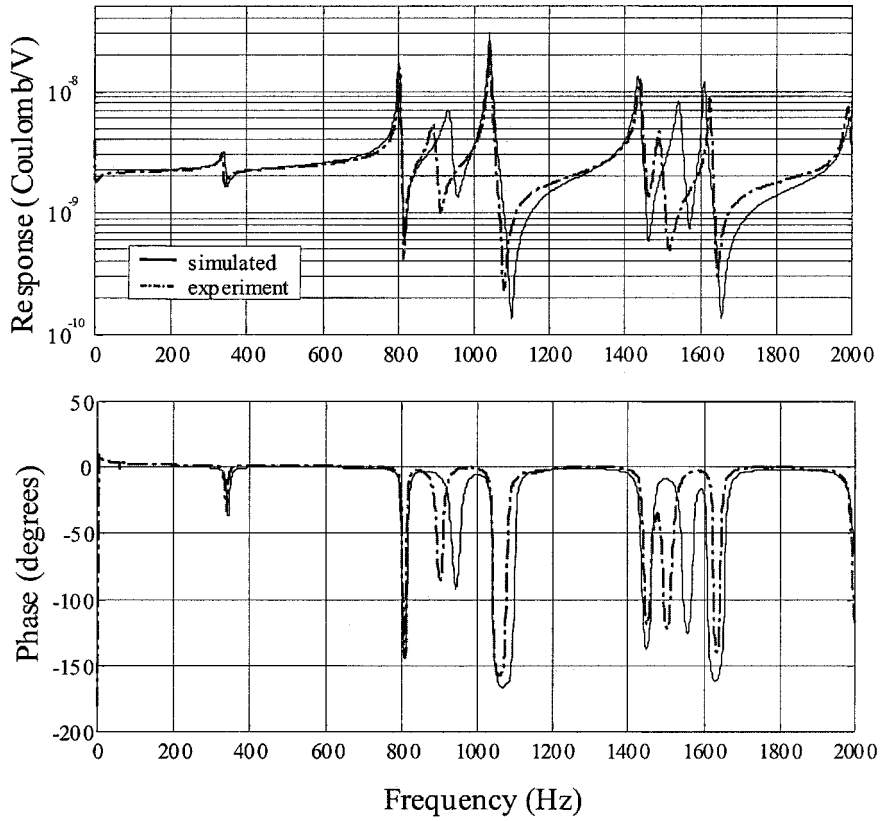

Fig. 3 Collocated PZT sensor/actuator response.

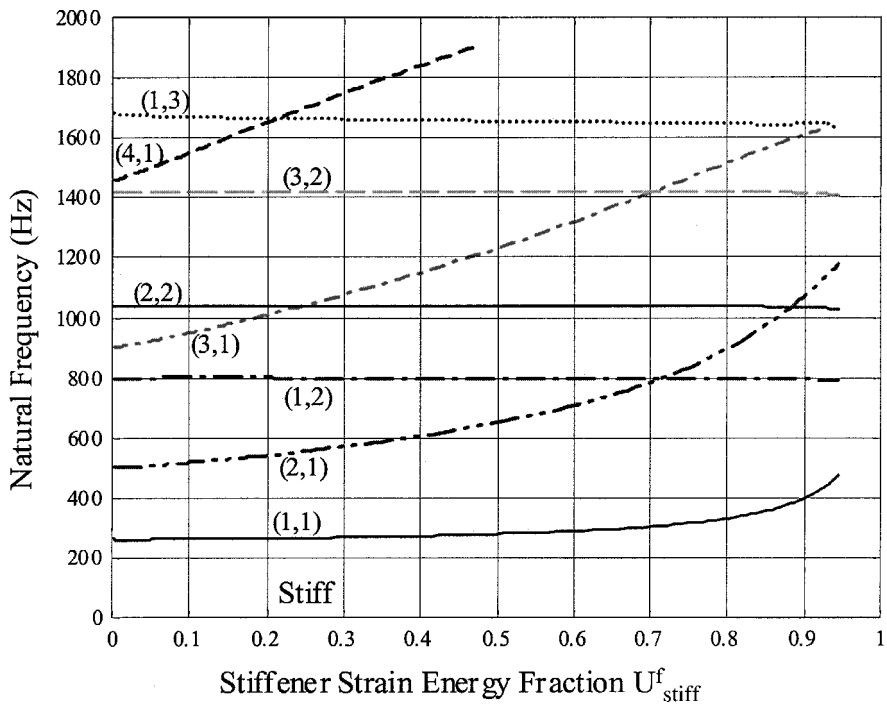

Fig. 4 Natural frequency of modes (by shape).

Also, the modal strain energy in the PZTs was nondimensionalized by dividing by the total modal strain energy (stiffened plate + PZTs). The nondimensional modal strain energy in the PZTs is denoted by U^f_{PZT}.

Natural Frequency

The natural frequencies of the first seven modes were calculated as the stiffener height h_{stiff} was varied from 0.25 to 25.4 mm with a stiffener thickness (t_{stiff}) of 1.59 mm. The natural frequencies of each mode shape are plotted vs the stiffener strain energy fraction U^f_{stiff} in Fig. 4. The stiffened plate mode shapes were identified by calculating the dot product between the predicted shape of each stiffened plate mode with the mode shapes of an unstiffened, simply supported plate.

The natural frequencies of the modes with shapes $(x,1)$ increased significantly with increasing stiffener height, whereas the other natural frequencies changed little. This result is explained by the fact that $(x,1)$ shapes involve significant bending of the stiffener, whereas

the other mode shapes do not. As the stiffener height is increased, the stiffener bending increases the stiffness for the $(x,1)$ modes while having little effect on the stiffness for the other modes.

PZT Coupling and Mode Shape Transition

The ability of surface-bonded PZTs to couple into the stiffened plate vibration was investigated for two PZT locations and a range of stiffener heights h_{stiff}. This coupling, which is a factor in determining the effectiveness of a PZT as a transducer, was quantified by calculating the modal strain energy fraction in the PZTs (U^f_{PZT}) for each mode. The magnitude of U^f_{PZT} indicates the potential effectiveness of the PZT as an actuator for either passive or active vibration control. Modal strain energy is not always a good indicator of the PZT coupling for modes in which the PZT is near a nodal line because the PZT charge is also affected by the sign of the curvature.[12] The studies described next are for a $3.18 \times 203.2 \times 304.8$ mm plate (the same dimensions as the experimental plate) and a 1.59-mm thick stiffener.

Figure 5 shows a plot of PZT modal strain energy fraction U^f_{PZT} for collocated PZTs (one PZT on each side of the plate) located at the center of one of the plate quadrants (quad PZT), as shown in Fig. 2. Figure 6 shows a plot of the PZT modal strain energy fraction U^f_{PZT} for collocated PZTs located at the center of the plate (center PZT). In both figures the curves are identified by the order in which the modes

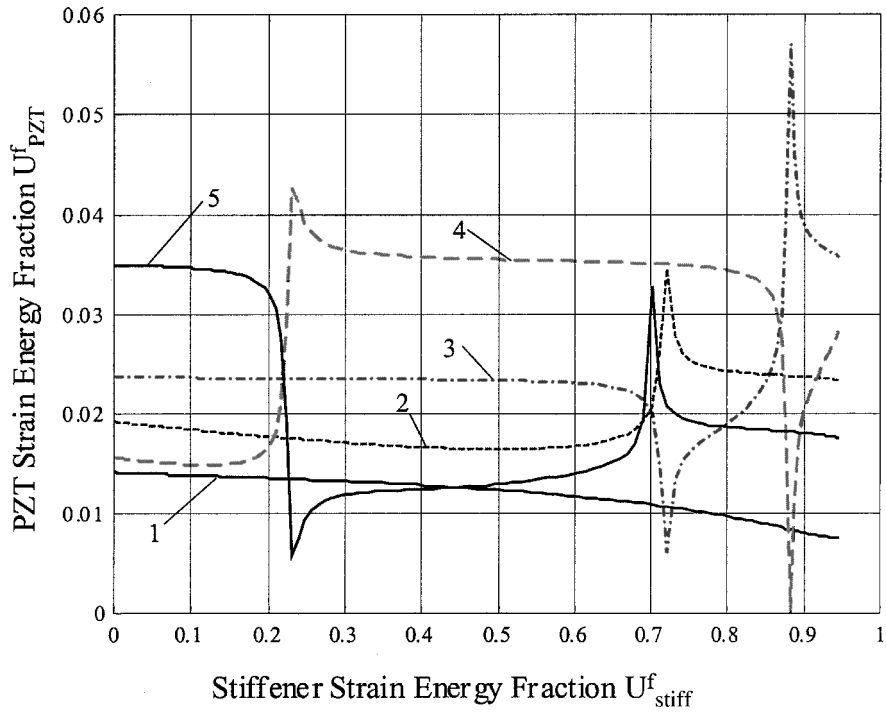

Fig. 5 PZT modal strain energy fraction for quadrant PZT.

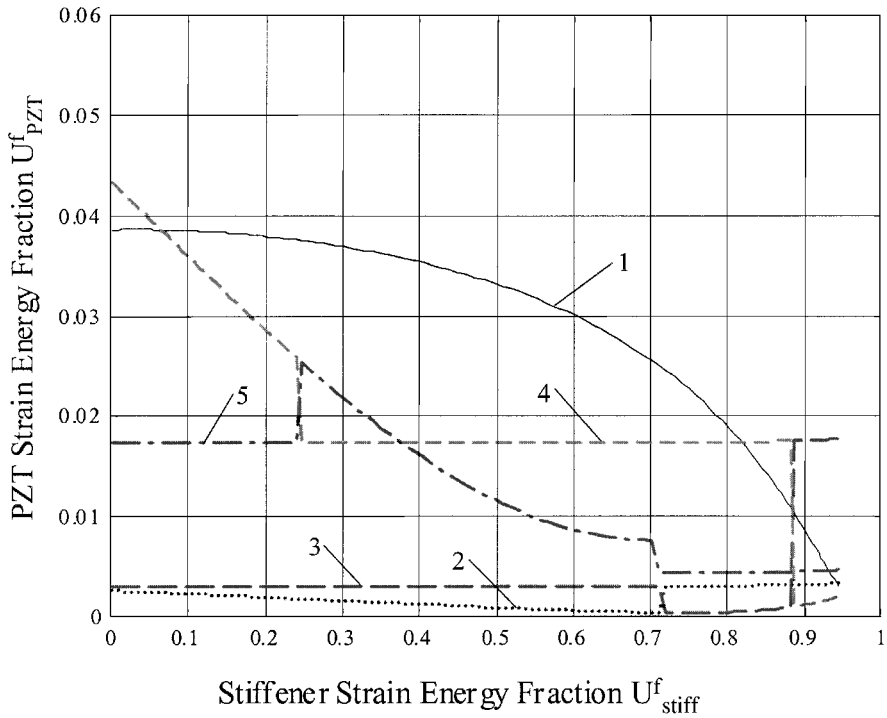

Fig. 6 PZT modal strain energy fraction for center PZT.

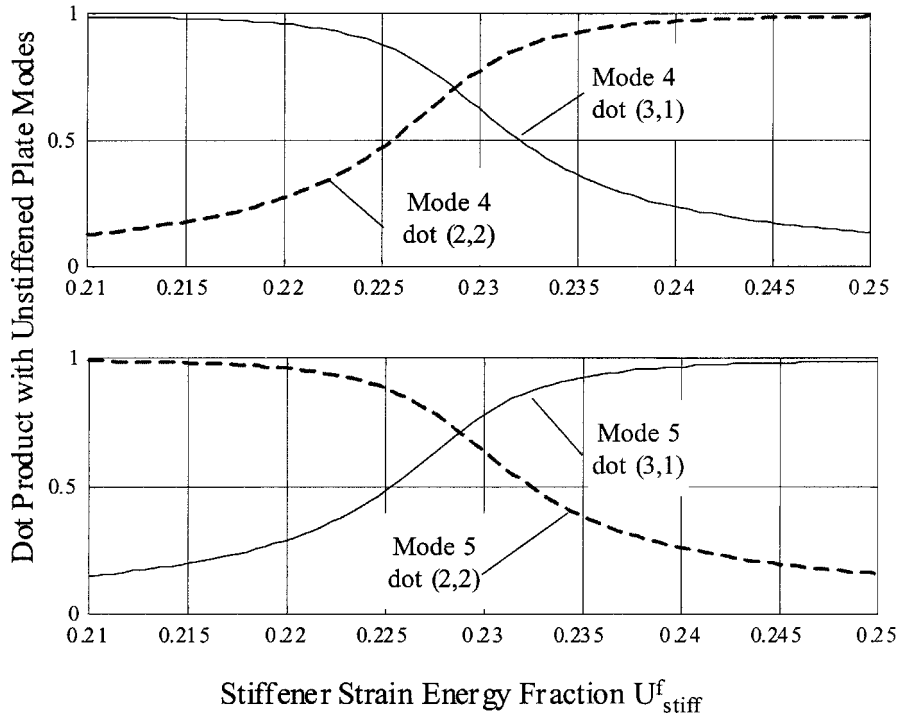

Fig. 7 Dot product between fourth and fifth modes of stiffened plate (with quadrant PZT) and unstiffened plate (2,2) and (3,1) modes.

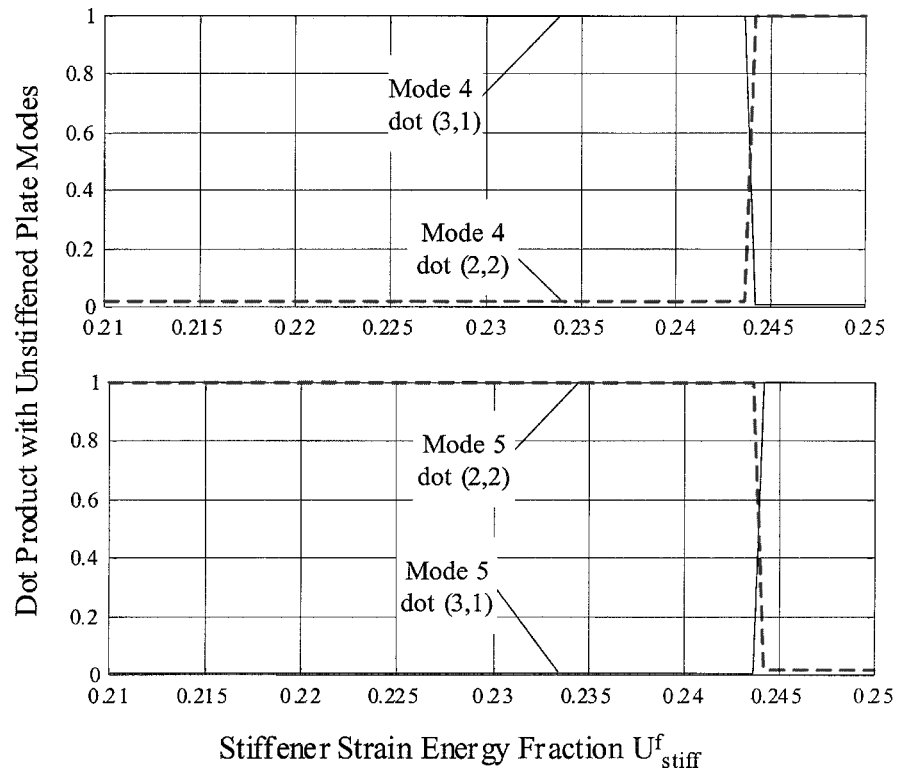

Fig. 8 Dot product between fourth and fifth modes of stiffened plate (with center PZT) and unstiffened plate (2,2) and (3,1) modes.

appear (frequency-wise). An interesting feature of the quad PZT plot is the presence of regions with large changes in strain energy with only a small change in stiffener height. These large changes in PZT strain energy correspond to modes with nearly identical natural frequencies (repeated eigenvalues). In this small range of stiffener heights, the order in which the mode shapes appear changes. These large changes in PZT modal strain energy do not appear in Fig. 6, the center PZT strain energy plot.

A more thorough investigation of one of these "transition regions" was conducted for the range of stiffener heights in which the order of the (3,1) and (2,2) modes changes. Figures 7 and 8 contain plots of the dot products between the fourth mode of the unstiffened plate and the (3,1) and (2,2) modes of a simply supported unstiffened plate, and between the fifth mode of the stiffened plate and the (3,1) and (2,2) unstiffened plate modes. Figure 7 corresponds to the stiffened plate with the quadrant PZTs, and Fig. 8 corresponds to the stiffened plate with the center PZTs. The stiffener thickness is 1.59 mm, and the stiffener height ranges from 5.18 to 5.69 mm. The transition in the order of the modes occurs over a much wider range of stiffener heights in the presence of the quadrant PZT. There is a

range of stiffener heights for which each of the stiffened plate (with quadrant PZTs) mode shapes resemble both the (3,1) and the (2,2) modes. A plot of the fourth and fifth mode shapes corresponding to a stiffener height in the transition region is shown in Fig. 9 (for the stiffened plate with quadrant PZTs). Figure 9 also contains a plot of the quadrant of the plate in which the PZTs are centered. It is the significant change in the curvature of these plate regions as the stiffener height is varied that causes the large change in modal PZT strain energy in the transition region. The fraction of modal strain energy in the PZTs is plotted in Fig. 10 for the fourth and fifth stiffened plate modes for the range of stiffener heights in which their natural frequencies are close.

One conclusion that can be drawn from this examination of the transition region is that for stiffener dimensions that result in nearly repeated eigenvalues the eigenvectors corresponding to those eigenvalues are relatively sensitive to small changes in the structure. This sensitivity will create difficulties in accurately predicting the effectiveness of surface bonded PZTs. This sensitivity only appeared in the case of a structure with an added asymmetry, the quadrant PZTs. The symmetric structure, the stiffened plate with center PZTs, did not have a range of stiffener heights with "distorted" mode shapes.

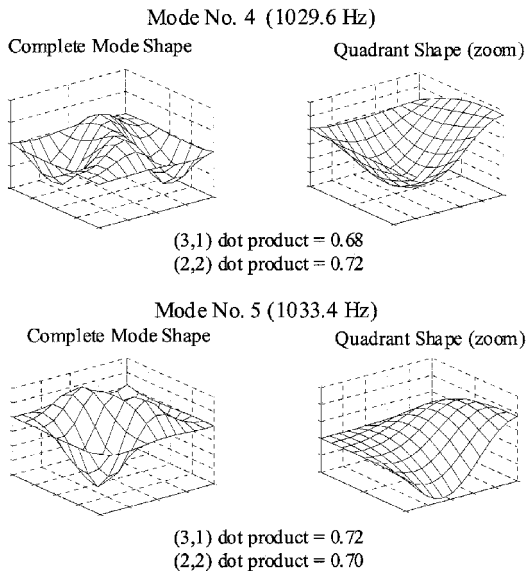

Fig. 9 Mode shapes in the transition between the (2,2)/(3,1) modes.

Summary

A Rayleigh–Ritz model of stiffened plates incorporating piezoceramic sensors and actuators was developed. The model includes the effects of multiple stiffeners and multiple piezoceramic elements. Clearly delineating the mass and stiffness matrix contributions of the various components, the model can easily be used to analyze the structural dynamics over a range of plate and stiffener parameters.

The model was correlated with experiments on an aluminum plate with one eccentric stiffener and simply supported boundary conditions. Both the natural frequencies and the mode shapes of the stiffened plate were accurately predicted. Frequency response analyses showed good agreement between simulated and experimental results for a collocated PZT sensor-actuator pair.

The model was used to investigate the changes in the dynamics of a rectangular plate with a single stiffener and surface-bonded PZTs for a range of stiffener heights. As expected, the natural frequencies corresponding to mode shapes that included significant strain of the stiffener increased while the other natural frequencies varied only a little. Also, for geometries with slight asymmetries and near repeated eigenvalues, the shapes of the modes corresponding the those eigenvalues appeared to be very sensitive to small changes in stiffener height. In the structure examined in this paper, the asymmetry was caused by a pair of collocated PZTs located in the center of one of the plate quadrants. The sensitivity of the mode shapes caused the PZT modal strain energy fraction for the fourth mode to increase by 140% with only an 8% increase in stiffener height. Over the same range of stiffener heights, the PZT modal strain energy fraction for the symmetric structure's fourth mode only changed by 5%. In general, this sensitivity can create difficulties in accurately predicting PZT coupling for modes whose natural frequencies are close to one another.

Future work can include experimental verification of the mode shape sensitivity with repeated eigenvalues. Also, the effects of other asymmetries (mass loading for example) can be explored.

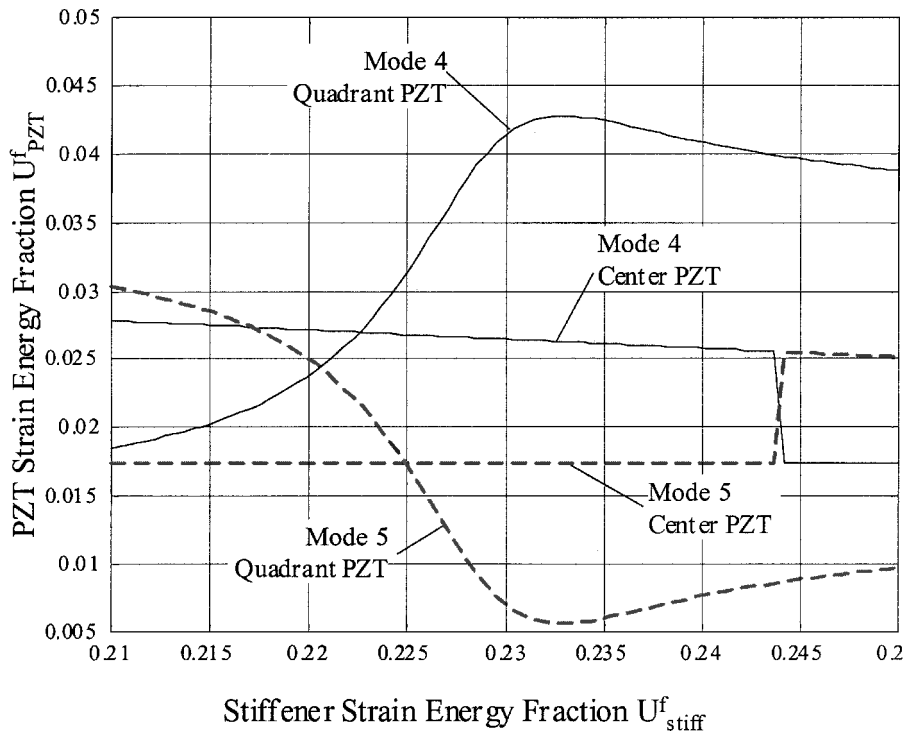

Fig. 10 PZT modal strain energy fraction near (2,2)/(3,1) mode transition.

References

[1]Kirk, C. L., "Natural Frequencies of Stiffened Plates," *Journal of Sound and Vibration*, Vol. 14, No. 4, 1970, pp. 375–388.

[2]Laura, P., and Gutierrez, R., "Transverse Vibrations of Rectangular Plates Elastically Restrained Against Rotation Along the Edges with Varying Stiffener Length," *Journal of Sound and Vibration*, Vol. 101, No. 1, 1985, pp. 122–124.

[3]Aksu, G., and Ali, R., "Free Vibration Analysis of Stiffened Plates Using Finite Differnence Methods," *Journal of Sound and Vibration*, Vol. 48, No. 1, 1976, pp. 15–25.

[4]Bedair, O., "Analysis of Stiffened Plates Under Lateral Loading Using Sequential Quadratic Programming (sqp)," *Computers and Structures*, Vol. 62, No. 1, 1977, pp. 63–80.

[5]Mead, D., Zhu, D., and Bardell, N., "Free Vibration of an Orthogonally Stiffened Flat Plate," *Journal of Sound and Vibration*, Vol. 127, No. 1, 1988, pp. 19–48.

[6]Mukherjee, A., and Mukhopadhyay, M., "Finite Element Free Vibration of Eccentrically-Stiffened Plates," *Computers and Structures*, Vol. 30, No. 6, 1988, pp. 1303–1317.

[7]Olson, M., and Hazell, C., "Vibration Studies of Some Integral Rib-Stiffened Plates," *Journal of Sound and Vibration*, Vol. 50, No. 1, 1977, pp. 43–61.

[8]Rossow, M., and Ibrahimkhail, A., "Constraint Method Analysis of Stiffened Plates," *Computers and Structures*, Vol. 8, No. 1, 1976, pp. 51–60.

[9]Wallace, C., "Radiation Resistance of a Rectangular Panel," *Journal of the Acoustical Society of America*, Vol. 51, No. 3, 1972, pp. 946–952.

[10]Fuller, C. R., Elliot, S., and Nelson, P., *Active Control of Vibration*, Academic Press, London, 1996.

[11]Johnson, C. D., and Kienholz, D. A., "Finite Element Prediction of Damping in Structures with Constrained Viscoelastic Layers," *AIAA Journal*, Vol. 20, No. 9, 1981, pp. 1284–1290.

[12]Davis, C. L., and Lesieutre, G. A., "A Modal Strain Energy Approach to the Prediction of Resistively Shunted Piezoceramic Damping," *Journal of Sound and Vibration*, Vol. 184, No. 1, 1995, pp. 129–139.

[13]Crawley, E., and De Luis, J., "Use of Piezelectric Actuators as Elements of Intelligent Structures," *AIAA Journal*, Vol. 25, No. 10, 1987, pp. 1373–1385.

[14]Crawley, E., and Lazarus, K., "Induced Strain Actuation of Isotropic and Anisotropic Plates," *AIAA Journal*, Vol. 29, No. 6, 1989, pp. 944–951.

[15]Dimitriadis, E., Fuller, C., and Rogers, C., "Piezoelectric Actuators for Distributed Vibration Excitation of Thin Plates," *Journal of Vibration and Acoustics*, Vol. 113, No. 1, 1991, pp. 100–107.

[16]Charette, F., and Berry, A., "Dynamic Effects of Piezoelectric Actuators on the Vibrational Response of a Plate," *Journal of Intelligent Material Systems and Structures*, Vol. 8, No. 6, 1997, pp. 513–524.

[17]Hagood, N., Chung, W., and von Flotow, A., "Modeling of Piezoelectric Actuator Dynamics for Active Structural Control," *Proceedings of the AIAA/ASME/ASCE/AHS/31st Structures, Structural Dynamics and Materials Conference*, AIAA, Washington, DC, 1990, pp. 2242–2256.

[18]Zhou, S., Liang, C., and Rogers, C., "A Dynamic Model of a Piezoelectric Actuator Driven Thin Plate," *Proceedings of the Society of Photo-Optical Instrumentation Engineers Conference on Smart Structures and Materials*, Vol. 2190, edited by N. W. Hagood, Society of Photo-Optical Instrumentation Engineers, Bellingham, WA, 1994, pp. 550–562.

[19]Zhou, S., Liang, C., and Rogers, C., "An Impedance-Based System Modeling Approach for Induced Strain Actuator-Driven Structures," *Journal of Vibration and Acoustics*, Vol. 18, No. 3, 1996, pp. 323–330.

[20]Meirovitch, L., *Principles and Techniques of Vibration*, Prentice–Hall, Upper Saddle River, NJ, 1997, p. 84,438.

[21]Harik, I., and Guo, M., "Finite Element Analysis of Eccentrically Stiffened Plates in Free Vibration," *Computers and Structures*, Vol. 49, No. 6, 1993, pp. 1007–1015.

[22]Blevins, R. D., *Formulas for Natural Frequecies and Mode Shapes*, Krieger, Malabar, FL, 1995, p. 278.

[23]Szilard, R., *Theory and Analysis of Plates*, Prentice–Hall, Upper Saddle River, NJ, 1974.

[24]Saada, A. S., *Elasticity: Theory and Applications*, 2nd ed., Krieger, Malabar, FL, 1993, p. 521.

A. M. Baz
Associate Editor